Molecular Imaging in Oncology

Document status and date:
Published: 01/01/2020

Document Version:
Publisher's PDF, also known as Version of record

Document license:
Taverne

Please check the document version of this publication:

• A submitted manuscript is the version of the article upon submission and before peer-review. There can be important differences between the submitted version and the official published version of record. People interested in the research are advised to contact the author for the final version of the publication, or visit the DOI to the publisher's website.
• The final author version and the galley proof are versions of the publication after peer review.
• The final published version features the final layout of the paper including the volume, issue and page numbers.

Link to publication

Download date: 02 May. 2024

Molecular Imaging in Oncology: Advanced Microscopy Techniques

16

Dimitrios Kapsokalyvas and Marc A. M. J. van Zandvoort

Contents

D. Kapsokalyvas · M. A. M. J. van Zandvoort (✉)
School for Oncology and Developmental Biology GROW and School for Cardiovascular
Diseases CARIM, Maastricht University, Maastricht, The Netherlands
e-mail: mamj.vanzandvoort@maastrichtuniversity.nl

D. Kapsokalyvas · M. A. M. J. van Zandvoort
Institut für Molekulare Kreislaufforschung, Universitätsklinikum Aachen, Aachen, Germany

16.1   Introduction

As the field of oncology is expanding, new processes are revealed, and many more questions arise. Investigation at subcellular resolution is not possible in the clinical setting, and therefore a preclinical platform is needed. This is offered by the use of immortalized cell lines where cellular and molecular dynamics can be investigated. However, it is often criticized that such cell lines resemble the clinical malignant tissue only to a limited extend. To address this issue, the use of small animals has been increasingly employed in oncology studies. This includes the use of wild but also transgenic species, modified to investigate the effect of different factors in oncological development or processes. Sample analysis can be done using molecular techniques, such as western blots, HPLC, mass spectroscopy, or through visualization using microscopy.

Imaging of tissue or cells with subcellular resolution is important for delineating molecular processes. Techniques that offer this kind of information include optical microscopy techniques (wide-field fluorescence, confocal laser scanning microscopy—CLSM, super-resolution microscopy—SRM, and two-photon laser scanning microscopy—TPM), and electron microscopy techniques (TEM, AFM, SEM, etc.). In this chapter, we will review only advanced optical fluorescence techniques since they are minimally invasive or non-invasive and require minimal sample preparation. Moreover, as it will be shown below, some of these techniques can be also applied in vivo offering a unique tool for investigating tumour dynamics and processes.

A plethora of techniques that offer resolution around 1 μm or better and are fluorescence-based is available. Each of them offers unique advantages. We will review the potential of each technique and highlight their strengths. These techniques include confocal laser scanning microscopy (CLSM), light-sheet microscopy (LSM), two-photon microscopy (TPM), and super-resolution microscopy (SRM) techniques.

16.2 Fluorescence and Labelling

Fluorescence-based microscopy techniques use the phenomenon of fluorescence as contrast mechanism. Fluorescence occurs when an excited molecule transitions from the first excited electronic state to the ground electronic state by emitting a photon. There are also other de-excitation mechanisms which are radiationless; therefore, they do not contribute to fluorescence. In fluorescence-based microscopy techniques, molecules with high fluorescence rates are used. In such techniques usually, excitation is accomplished with a laser line. A typical Jablonski diagram of de-excitation transitions of the microscopy techniques described in this chapter is depicted in Fig. 16.1. Traditional bright-field microscopy, as the one used for histopathologic examination of tissue slides, relies on the phenomenon of absorption or scattering for contrast. This limits the number of contrast agents, as absorption spectra are generally broad and overlap, and additionally out of focus signal significantly blurs the image. In fluorescence, emission spectra are generally narrower, since only two electronic states are involved in the process. As a result, it is easier to control excitation and detection, by using a specific excitation wavelength for each fluorophore and selecting only a small wavelength bandwidth for detection. In this way, three or more fluorophores can be combined in a single sample and the excitation of each fluorophore can be controlled independently. Conventional wide-field fluorescence microscopy is not reviewed in this chapter as it offers lower axial resolution compared to the other techniques.

In microscopy, fluorescence is used to increase contrast. In order to achieve this contrast, the structure under investigation, e.g. a protein, DNA, has to be labelled with a fluorescent marker. To achieve this, several methods for labelling have been developed.
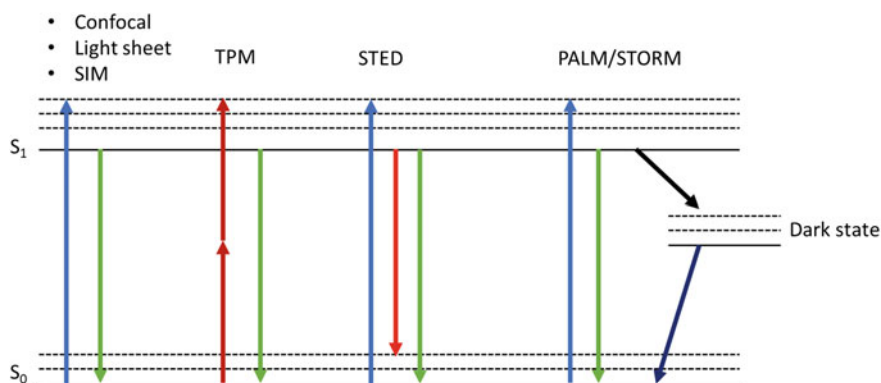

Fig. 16.1 Jablonski diagram of the molecular transitions of fluorophores in different microscopy techniques

16.2.1 Chemical Labelling

In this case, a molecule, a peptide, or a chemical agent in general that is shown to preferentially bind to a specific structure is used for direct labelling. When the chemical agent is not fluorescent itself, it is conjugated to a fluorescent dye. Examples of such agents include DAPI and Hoechst, commonly used for nuclear staining. Other examples are specific mitochondrial dyes (such as Mitotracker, TMR, or JC-1, the latter with fluorescence colour depending on mitochondrial membrane potential), actin dyes (such as phalloidin or SiR-actin), or membrane dyes (such as DiI, WGA, and MemBrite). This kind of labelling is relatively easy and usually requires a single step of incubation, after which the labelled structure becomes visible on a dark background.

16.2.2 Immunofluorescence

Immunofluorescence staining involves the use of antibodies that target specific proteins in the cell. The primary antibody can be linked to a fluorescent probe directly. More commonly, a secondary antibody carrying the probe (usually organic dyes) is used to target the unlabelled primary antibody. In the case of using secondary antibodies, more than one secondary antibody can bind to the primary antibody, therefore increasing the fluorophore density, and thereafter signal. The advantage of antibody labelling is that any structure in the cell can be specifically labelled. The disadvantage, however, is that it can only be performed on fixed samples. Antibody labelling, in general, is a multistep process that requires fixation, permeabilization, and staining of the sample, and several washing cycles in between. In intact tissues and living animals, the antibodies cannot penetrate deep enough. They can certainly not enter intact cells, allowing only labelling of external targets.

To address issues concerning the size of conventional antibodies especially in applications of super-resolution microscopy, new generation of markers has been developed. These include affibody proteins [1], which are small synthesized peptides designed to target a specific protein, and antibody fragments [2], which are engineered to retain the targeting properties of the full antibody but be smaller in size. One could also consider chromobodies as an example of this type of staining, since the cell is transfected with the heavy chain fragment of a lama antibody to a specific protein. Such staining agents can either be conjugated to a fluorophore or be followed by an additional step of secondary labelling, similar to classical immunostaining.

16.2.3 Fluorescent Proteins

In this case, the DNA of the host is modified to express a fluorescent protein (FP) such as green fluorescent protein (GFP), and yellow fluorescent protein (YFP) in the target structure. This can be achieved temporarily by transfecting the

cell with a plasmid that contains the FP's DNA. Transfection efficiency can vary due to competing mechanisms in the cell and as a result transfection efficiency can vary significantly from cell to cell. To address this issue, the DNA of the host can be modified permanently to express the FPs. The later method is more challenging to achieve but offers more reliable results. It can be performed on cell lines or even small animals such as mice, rats, and zebrafish. FPs are not as bright as organic dyes; however, they are expressed specifically on the desired target (e.g. a protein like LaminA, Actin). Furthermore, since they are expressed naturally by cells, FPs are optimal for live-cell imaging.

In more advanced applications where signal intensity is important for applications, such as live-cell imaging or single-molecule microscopy, the so-called SNAP [3], Halo-, and CLIP-tag methods can be used [4]. These are self-labelling enzymes which can be fused to a target protein and can covalently bond to a labelled ligand. The advantage of this method is that organic dyes can be used for ligand labelling, which are brighter than FPs.

16.2.4   Photo-Switching Dyes

Photo-switching dyes are used in super-resolution techniques. SRM techniques rely on their ability to drive the dye in states that are fluorescent—the ON state—and states that are non-fluorescent—the OFF state—in a controlled manner [5] (Fig. 16.1). This includes dyes that can reversibly photoswitch between an OFF and ON state (such as cis-trans isomerization of FPs, or dyes in the presence of strong reducing solutions [6]), dyes that irreversibly photoswitch from an OFF state to an ON state, and dyes that are irreversibly photoconverted from one fluorescence state to another red-shifted fluorescence state. Their emission state can be controlled, and the emission from a single molecule can be recorded independently of neighbouring molecules. This method provides a detailed and high-resolution "map" of each fluorophore. Such dyes are commonly used in PALM/STORM-related techniques.

16.3   Fluorescence Microscopy Techniques

In this chapter, we will discuss the most frequently used microscopy techniques in oncological research. We refer to Fig. 16.2 for a detailed schedule of the individual setups.

16.3.1   Confocal Microscopy

Confocal laser scanning microscopy (CLSM) was conceptualized in the late 60s; however, it became widely applicable in the late 80s and early 90s. Developments in laser technology and electronics allowed the construction of electronic microscopes.
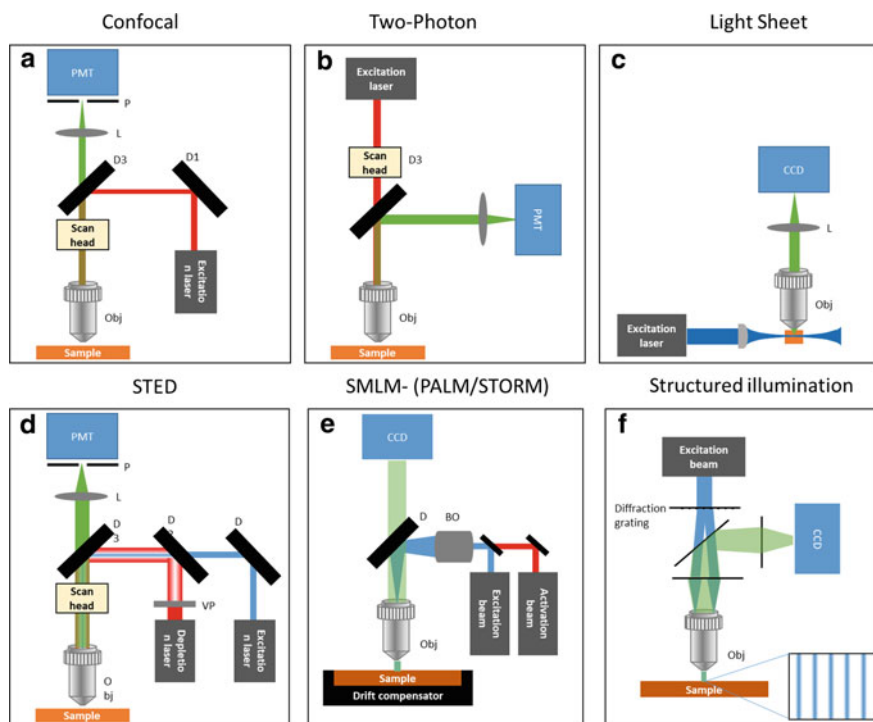
Fig. 16.2 Schematic overview of different fluorescence microscopy techniques. **a** Confocal microscopy, the sample is scanned with a laser source and fluorescence is detected by a photon detector PMT. Out of focus light is rejected by the pinhole (P). **b** Two-photon microscopy, a pulsed near-infrared laser source is scanning the sample and a PMT is detecting the signal. **c** Light-sheet microscopy, a sheet of light excites the sample from the side and a perpendicularly positioned objective lens is collecting fluorescence to form the image on the CCD or sCMOS camera. **d** STED, it is a confocal-based method where additionally a depletion beam is scanning the sample along with the excitation beam. **e** SMLM, activation and excitation beams are used at different frequencies and intensities to drive molecules stochastically in and out of the fluorescence state. **f** SIM, a diffracting element is used to create a striped illumination pattern at the focal point. This pattern is rotated, and subsequent images are post-processed

Combined with the use of a high intensity collimated light source—the laser—and multiple electronic systems that could be synchronized and controlled by a computer, this allowed the production of high-resolution tomographic images. Nowadays, confocal microscopy is a standard technique for light microscopy facilities [7]. Contrast is based on fluorescence and any conventional dye (using the labelling techniques described above) can be used for imaging. A pinhole is used to reject the out of focus light and restrict the axial dimensions of the section being imaged. Such detection requires high levels of signal, since signal mainly form the focal spot that is mainly collected; therefore, in practice modern bright dyes that are less sensitive to photobleaching are favoured. Typically, resolution in confocal microscopy is around

250 nm in XY and 700 nm in axial dimension. Confocal microscopy can be used for imaging of any type of cell process in culture, in both fixed and living cells. It can also be used as an alternative to histopathology, where biopsies can be imaged immediately after removal in order to define tumour margins and type [8]. The advantage is the 3D sectioning and higher resolution compared to conventional wide-field microscopy. Contrast and resolution of confocal images can be further improved by post-processing based on deconvolution algorithms. This technique is very efficient in reducing noise and enhancing contrast of subtle structures, therefore increasing resolution, especially in "noisy" images [7].

16.3.1.1 Limitations

Confocal microscopy uses visible light for excitation. Visible light has low penetration depth; therefore, thicker tissues cannot be visualized. Penetration depends on the sample absorption and scattering properties, and typically is in the 50–100 μm range. At deeper layers, out of focus fluorescence cannot be rejected anymore, due to scattering, and images become blurry. Another limitation is the number of fluorescent probes that can be used. Commonly, three different probes can be used without complications, using sequential imaging. Use of more probes is possible, though the risk of fluorescence cross-talk from one channel to the other increases. Because it is a scanning technique, it is slower compared to conventional wide-field fluorescence. To increase scanning speed resonant scanners can be used, which can acquire images at video rate (30 frames per second-fps) with good signal-to-noise ratio (SNR). Another application which can increase acquisition speed is the *spinning disc confocal*. In this case, instead of scanning the laser beam over the sample, two discs, one containing microlenses and the other individual pinholes, are rotated in tandem to scan the sample, and the image is projected on a camera such as a CCD or sCMOS. Spinning disc offers high-speed scanning, but resolution is inferior to classical CLSM due to pinhole cross-talk.

16.3.2 Light-Sheet Microscopy—LSM

Light-sheet microscopy (LSM) or selective plane illumination, a technique recently introduced [9, 10], has received a lot of attention. Light sheet, instead of using the same path for excitation and detection as in CLSM and TPM, uses a thin sheet of light to excite a layer of the sample. Another objective placed perpendicular to the excitation light sheet is used to collect the generated signal. By doing so, the entire illuminated (and excited) section of the sample can be used to collect signal from. Since there are full field excitation and image formation, LSM is very fast. Its resolution is mainly dependent on the thickness of the light sheet, typically being in the 1–2 μm range. The extension of the light sheet over which it can maintain a relative homogeneous thickness defines the maximum field of view, typically around 0.5–1 mm. LSM typically offers less resolution compared to CLSM and TPM, but it is much faster (several frames per second) and allows imaging of large

fields of view. However, samples need to be transparent, for example, embryos (such as drosophila, zebrafish), and small organoids, and cleared organs [11].

Recently, super-resolution variations of LSM, such as lattice light sheet, have been reported, which offer reduced field of view and penetration depth but are significantly fast [12]. Also, a non-invasive in vivo application was presented, which gives promise for further development of the intravital application of the technique [13]. This opens up the potential for intravital imaging also in oncology with very high-resolution and video-rate acquisition.

16.3.2.1 Limitations

Because of its orthogonal excitation detection geometry, LSM poses limitations on the objectives that can be used and on the sample positioning in the microscope. In routine applications, resolution is inferior to that of CLSM or TPM; therefore, if the structure of interest is below the 1 μm range, super-resolution techniques will have to be preferred instead. Additionally, penetration depth can be a concern; therefore, if the tissue is not transparent, either naturally (embryos) or by clearing, penetration is limited in the 50–100 μm range depending on the sample.

16.3.3 Two-Photon Microscopy

Two-photon microscopy (TPM) (also referred to as two-photon excitation, two-photon laser scanning, multiphoton, or non-linear microscopy) was invented in the early 90s [14]. Its development was facilitated by the presence of very fast laser-pulsed systems (80 MHz) able to deliver very short pulses in the range of hundreds of femtoseconds with high enough intensity. Because light scattering and absorption in biological samples for the near-infrared laser sources (usually 740–860 nm) used in two-photon microscopy is much lower than that for the visible spectrum, near-infrared light can penetrate deeper. This property allows high-resolution imaging deep in tissue sections, organs, and organisms in vitro and in vivo. The actual penetration depth depends on the optical properties of the tissue and can range from 200 μm [15] in skin up to 1 mm in brain [16]. Additionally, due to the fact that excitation takes place only in the focal plane, a pinhole is not needed. Therefore, detectors can be placed closer to the sample and as a result detection can be more efficient. Like confocal microscopy, it is a scanning technique and again similar to confocal can produce 3D images. Resolution in TPM on very thin samples, such as cells or surface of tissues, is worse than confocal due to the longer excitation wavelength used. However, at deeper layers, confocal resolution worsens significantly due to scattering, while in TPM resolution is less affected (since fluorescence originates from the focal spot), so as a result resolution of TPM becomes better compared to confocal at deeper layers. Since in TPM excitation only takes place in the focus of the objective, photobleaching and photodamage are overall less compared to that in confocal microscopy. However, photobleaching rate can be significantly higher in the focus, compared to confocal, due to non-linear processes [17].

Typically, in TPM, objectives with lower numerical aperture (0.8–1 NA) and low magnification (20X) are used. Such objectives offer bigger field of view (500–700 µm), have longer working distances (2–8 mm), and are water immersion. This facilitates the application of tissue imaging where deeper penetration is needed, water immersion is more compatible with tissues, especially when doing intravital imaging, and capturing as more as possible of bigger morphological structures is required. Resolution for such objectives is around 500 nm in the lateral plane, and 1.5 µm in the axial direction.

Another advantage of TPM is that it can effectively excite and detect endogenous fluorophores as well as image collagen in the extracellular matrix based on the second harmonic signal (SHG). There are several natural fluorophores in tissue such as keratin, melanin, NDH, FAD, collagen, and elastin. These can be used to visualize tissue, which is usually termed as autofluorescence. In TPM, many probes and/or autofluorescent structures can be excited with a single wavelength (for example, 800 nm). This in contrast to the sequential imaging needed in CLSM. This is especially relevant in intravital imaging or in imaging in living cells. When considering intravital applications the advantage is that instead of UV light that would be required for one-photon excitation, such as in confocal microscopy, a near-infrared source is used which is not damaging DNA. Additionally, the SHG of collagen is commonly used as a label-free method to image the extracellular matrix (collagen). Another tissue element that can emit SHG is striated muscle; however, it is not usually relevant in oncology.

Several reviews already exist on this topic [18–23]. In this section, we will review the most important applications.

16.3.3.1   Limitations

TPM can efficiently excite autofluorescent molecules of the samples but when exogenous labelling is used, autofluorescence can be a problem as it adds an unwanted fluorescence background. Protocols to decrease autofluorescence background have been proposed [24], but they do not apply for every tissue and are not applicable in vivo. Due to the NIR wavelength used for excitation, resolution is lower compared to CLSM.

16.3.4   Super-Resolution Microscopy Techniques

Key contributors to the development of super-resolution techniques have been awarded the Nobel prize in chemistry in 2014. The most common techniques are simulated emission depletion (STED), photo-activatable localization microscopy (PALM), stochastic optical reconstruction microscopy (STORM), and structured illumination microscopy (SIM).

STED

STED is a confocal-based technique that additionally employs a depletion beam (usually in the red-infrared spectrum) to eliminate fluorescence emitted around the central point of excitation. This reduces the excitation region leading to improved resolution [25]. Resolution can be tuned by adjusting the depletion beam intensity according to the fluorophore, and the sample's properties. In biological specimens, resolution can be down to 70 nm in XY- and Z-directions. Since it is confocal-based method, it can offer sectioning capabilities and 3D imaging up to 50 μm in the sample, especially with refractive index correction objectives. Also, compared to other super-resolution techniques, it is fast (20 images per second in resonant scanner mode) and no post-processing is needed. Consequently, it can be used to study dynamic processes in living cells. Resolution in STED depends on the intensity of the depletion beam. Therefore, resolution can be tuned according to the desired resolution or the (bleaching) properties of the fluorophore.

16.3.4.1 Limitations

In STED, two laser beams are applied, one in the visible spectrum for excitation and another in the red-infrared spectrum for depletion. Usually, high levels of light are used for the depletion. This can lead to fast photobleaching of the sample. Therefore, dyes that are very photostable and bright are needed. Furthermore, an absolute prerequisite is that the probe does not absorb at the depletion wavelength. Imaging deeper sections of the sample are possible; however, penetration depth is similar to that of confocal and limited to 50–100 μm depending on the sample properties.

16.3.5 Single-Molecule Localization Microscopy—SMLM

Single-molecule localization microscopy (SMLM) techniques, such as PALM [26] and STORM [27], rely on determining the exact localization of a fluorophore in the sample. This is achieved by means of stochastic excitation of a subset of fluorophores. Comparing with conventional fluorescence microscopy, fluorescence still takes place, but a "dark state" (a state from which the fluorophore cannot fluoresce) is also involved in the fluorophore transitions. In a typical SMLM experiment, all fluorophores are in a "dark state" and then with low-intensity light a subgroup is activated and transitions to the "bright state" in which the molecule can transition between the singlet electronic states and emit fluorescence as depicted in Fig. 16.1. After the fluorophore has emitted sufficient photons for accurate localization transition to the "dark state" or can be permanently turned off by photobleaching. It is a repetitive process, until all fluorophores have been sufficiently interrogated. The resulting image is a map of the localization of the fluorophores. Resolution depends on the density of the fluorophores and on the number of photons collected.

The density should be chosen in agreement with the size of the structure to be imaged. A pitfall in this case is that when the density is too high, the simultaneous activation of fluorophores within the same diffraction-limited volume can take place, resulting in artefacts. Also, dyes have limitations on the number of photons that they can emit before entering a non-fluorescent state. The typical resolution that can be achieved is in the range of 20–50 nm. Several variations of these techniques have been developed to improve speed, specificity, photon collection efficiency, and resolution

16.3.5.1   Limitations

SMLM techniques are rather slow; acquisition of a single final image is in the order of seconds in modern setups. This severely hampers the imaging of fast processes in living cells. Furthermore, only images up to a depth of 1 μm can be made (using special cylindrical lenses), excluding visualization of processes and morphology deeper in cells. Finally, only certain types of dyes in combination with dedicated mounting methods can be used.

16.3.6   Structured Illumination Microscopy—SIM

In structured illumination microscopy (SIM) [28, 29], the sample is illuminated with a pattern of alternating bright and dark stripes. This pattern is usually created by using a diffractive mask, or by using a spatial light modulator (SLM). This pattern is then rotated, and the acquired images are post-processed. This method of illumination creates the so-called Moiré fringes, highlighting sub-diffraction features. With post-processing of the images, the high spatial frequency components of the image (higher order details) are extracted, and consequently resolution is improved up to twofold (~ 120 nm). Further improvement in resolution can be achieved by modifications to this technique, i.e. Saturated SIM (SSIM) [30, 31]. Resolution improvement is limited compared to other super-resolution techniques, but advantages of SIM are that there are no specific requirements for the dye selection, so any conventional dye is adequate. Additionally, since excitation light is usually low in intensity, photodamage and photobleaching are reduced. SIM is most commonly applied to wide-field microscopes, but application to scanning microscopes is also possible. It can also be used for in vivo studies; however, images will require post-processing to extract super-resolution.

16.3.6.1   Limitations

Image acquisition involves the acquisition of several sequential images of the same region. When imaging dynamic processes, this can be an issue if the acquisition time is larger than the period of the process investigated. Moreover, images need to be processed in order to construct the final image, which increases the total imaging time and the processing needs of this technique. Resolution improvement is limited to up to twofold which is not as high as the other SRM techniques offer (STED: 70 nm, SMLM: 20 nm).

16.4   Applications

16.4.1   Confocal Microscopy

CLSM is one of the most common microscopy techniques used in life science, found in most research institutes. It has been used in numerous studies studying the molecular basics of cancer. The major advantages are that it can provide high-resolution tomographic images of cells and subcellular compartments. For example, it has been used for investigating tumour initialization and analysing stem cell dynamics where it was shown that evolution of malignant mutations is not deterministic and that also the environment can affect their evolution [32]. Confocal microscopy was also used to investigate the kinetics of tumour cells and the effect on DNA damage. It was shown that tumour cells can reshape in order to migrate through very small openings, and even though nuclear envelope can rapture during this process and sustain DNA damage, they have repair mechanisms [33]. Another example includes the use of confocal microscopy to investigate the cell renewal of cancer stem cells on organoids developed from patient cells and implanted on mice [34]. The parameters leading to tumour regression were also visualized with CLSM.

Similar to the CLSM method based on fluorescence, a sister technique based on reflection (Reflectance CLSM) from tissue has been developed. This method has found applications that are closer to the clinical setting as no staining is required, since signal originates from the reflectance signal of the tissue itself. It has been particularly useful in clinical applications of imaging skin lesions [35, 36]. Another example is the use of these techniques for imaging breast needle core biopsies [37] which could provide an alternative to the classical histopathologic investigation of biopsies (Fig. 16.3).

16.4.2   Light-Sheet Microscopy—LSM

LSM microscopy with tissue clearing techniques was used to image whole solid tumours with high resolution [38]. The phenotype and heterogeneity of solid tumours were visualized in terms of vascularization and vessel thickness. Moreover, cancer pattern heterogeneities regarding E-cadherin, N-cadherin, vimentin, and CD34 were also visualized. What was also important was that the tissue used was paraffin embedded and deparaffinized for imaging and afterwards reparaffinized for storage and future re-evaluation. This approach has the potential of more accurate identification of phenotypic patterns which can be discerned better in the 3D image compared to the 2D images of histopathology [39] (Fig. 16.4). Targeting at the diagnostic advantages that LSM can have over conventional histopathology, it was used to image thick histological sections (0.4 cm) of tissue. The advantages were that thick tissue slices could be imaged very fast, and structures of interest were not distorted due to μm slicing, as it could happen with conventional histopathology [40].
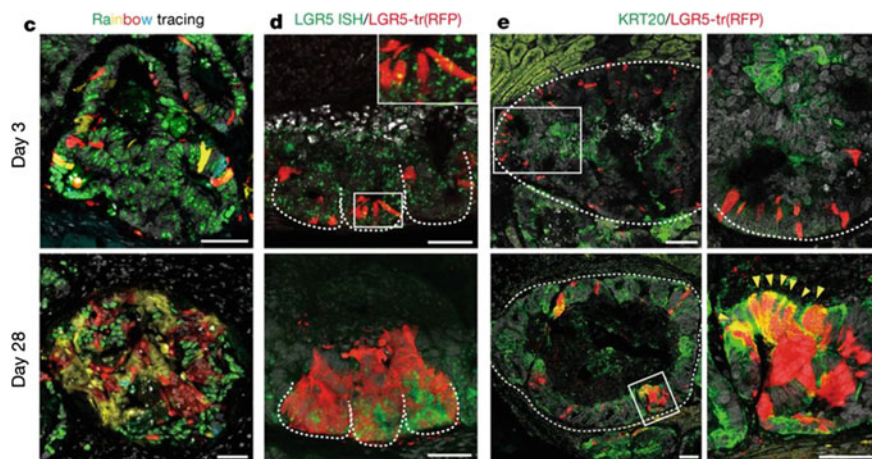
Fig. 16.3 Confocal images of cancer stem cell (LGR5-CreER) tracing in organoids. Cells have been modified to express different fluorescent proteins—nGFP (green), EYFP (yellow), CFP (cyan), and RFP (red). The results of treatment with tamoxifen after 3 days (upper row) and after 28 days (bottom row) are visualized. A number of clones have decreased after 28 days. Scale bars first, second, and fourth column: 50 μm, third column: 100 μm. Adapted from [34]
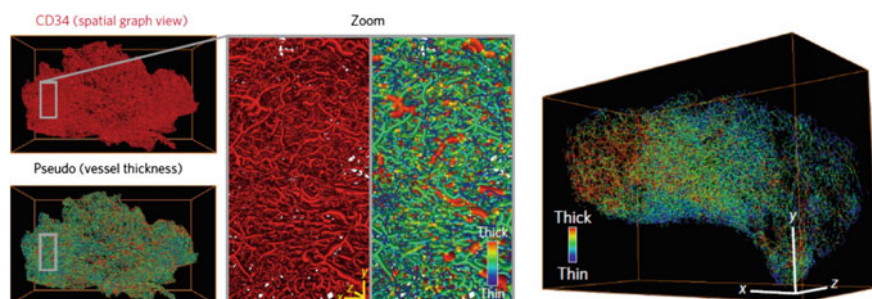
Fig. 16.4 LSM images of cleared human tumour sample. CD34 immunolabelling reveals the vasculature. In the zoom inset vessels are colour coded for different thicknesses (x, y, z indicators 80 μm). On the right, the entire reconstructed tumour sample with vessel thickness colour coding (x, y, z indicators, 100 μm). Adapted from [39]

16.4.3 Two-Photon Microscopy

16.4.3.1 Ex Vivo

Two-photon has been used to elucidate tumour molecular processes in various organs. It has often been used to compare histopathological results of standard H&E staining with those of TPM. Usually, TPM imaging is based on endogenous signal

of the tissue. Spectral properties that differentiate in malignant tissue are used for tumour identification and delineation. Examples include imaging of colorectal cancer tissue [41] where identification was based on nuclear size and collagen intensity, healthy bladder mucosa, and carcinoma in situ [42], where morphological and spectral emission differences between healthy and malignant lesions were identified, and in breast cancer [43]. Common findings in these cases were that nuclear morphology is irregular in malignant tissue, extracellular matrix organization is disrupted by tumour cells, and often spectral shifting is observed.

16.4.3.2 Metabolic Imaging

One of the advantages of endogenous fluorophore imaging is the ability to monitor the metabolic state of cells. This has been successfully used to monitor differences in metabolic activity of various grade cancer cells. The technique is based on measuring the autofluorescence levels of coenzymes that play key roles in the respiratory chain of cells, such as nicotinamide adenine dinucleotide (NADH) and flavin adenine dinucleotide (FAD) [44–46]. Cells produce energy in the form of ATP mainly through oxidation–reduction (redox) reactions, where NADH and FAD are involved. NADH and of FAD are autofluorescent, also under two-photon excitation at 740 nm and 820 nm, respectively [47]. Since they have distinct spectral emissions profiles, they can be separated, and their contribution measured. The ratio of their fluorescence intensities can be used to calculate the redox state of a cell. Increased ratio of FAD over NADH is associated with oxidative activity, whereas decrease of this ratio is correlated with glycolytic activity. These properties have been used to evaluate redox level in epithelial precancer cells [44] and breast cancer [48].

Other studies have focused on the fluorescence decay characteristics of NADH and FAD. More specifically, the reduced form of NADH fluoresces with a characteristic fluorescence lifetime depending on whether it is bound to a protein or free. The free form of NADH has a short fluorescence lifetime (0.4–0.8 ns) and is often associated with glycolytic activity. The bound form has a longer fluorescence lifetime (2–4 ns) and is associated with oxidative phosphorylation. The oxidized NAD^+ is not fluorescent. FAD is autofluorescent in a different emission range and when bound to a protein has a short fluorescence lifetime (0.8 ns), whereas when free has a long fluorescence lifetime (2.0 ns).

Changes in the mean lifetime of NADH have been observed in cancerous and precancerous cells [44] (Fig. 16.5), the proliferative state of the cell [49], the differentiation pathway of stem cells [50], or the cell response to toxic agents [51]. These reports suggest that the mean NADH lifetime is associated with the metabolic state of tissue. Since in cancer metabolism shifts towards anaerobic glycolysis (the Warburg effect), it is expected that this shift would be reflected in NADH lifetime. This technique has been used to identify precancerous epithelia [44], changes in bladder carcinoma in situ [42], and malignant skin lesions [52].
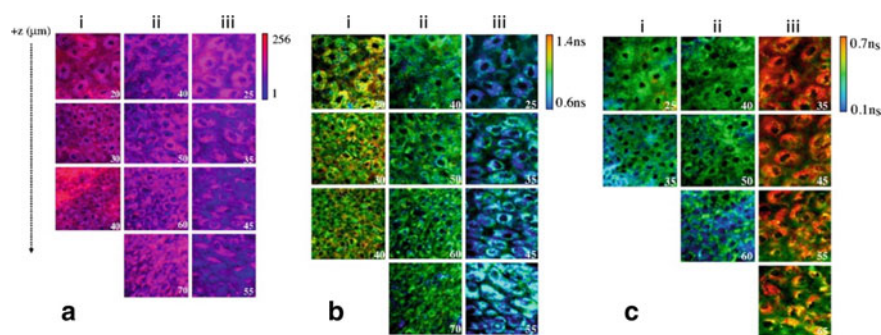
Fig. 16.5 **a** Redox ratio (FAD/NADH), **b** mean NAD lifetime, and **c** mean FAD lifetime of normal low-grade and high-grade precancer endothelial cells. Z-axis indicates depth inside the tissue. Adapted from [44]

16.4.3.3 Multiphoton Imaging of Skin

Skin, as it is the outermost human organ, is easily accessible for non-invasive imaging with TPM. For this reason, TPM has been particularly applied in imaging skin lesions in model organisms, such as mice [53] and ex vivo human biopsies [54], and later in human skin in vivo [15, 55].

In vivo application poses several limitations, most significantly the restricted use of light intensity in the order of 20–40 mW and absence of compatible in vivo labels. Skin imaging is therefore based completely on endogenous fluorophores. Luckily enough, there are several endogenous fluorophores present in skin [56, 57]. Most abundant are keratin, melanin, NADH, FAD, and lipofuscin in the epidermis, collagen, and elastin in the dermis. Detection of the endogenous signal is adequate to visualize cells and subcellular components, such as mitochondria. Usually, cell nuclei are identified as dark regions, since they don't exhibit autofluorescence, inside a bright autofluorescent cytoplasm. In the dermis, SHG from collagen and fluorescence from elastin offer a detailed view of the extracellular matrix morphology. Melanin is brightly fluorescent and can also be visualized in melanocytic skin lesions. Stratum corneum contains significant amounts of keratin and also lipofuscin. Changes in the morphology of skin lesions compared to normal skin, but also spectral and fluorescence decay properties of individual fluorophores, are used to identify and diagnose skin lesions. Advances in speed have allowed mesoscopic imaging of skin lesions [58] (Fig. 16.6).

TPM has been applied in imaging skin tumours, such as squamous cell carcinoma [59], basal cell carcinoma [60–62], and melanoma [63]. It was also shown that imaging of mitochondrial dynamics could be used for diagnosis of early-stage malignancies in vivo, based on the differences in mitochondria organization patterns [52] (Fig. 16.7).
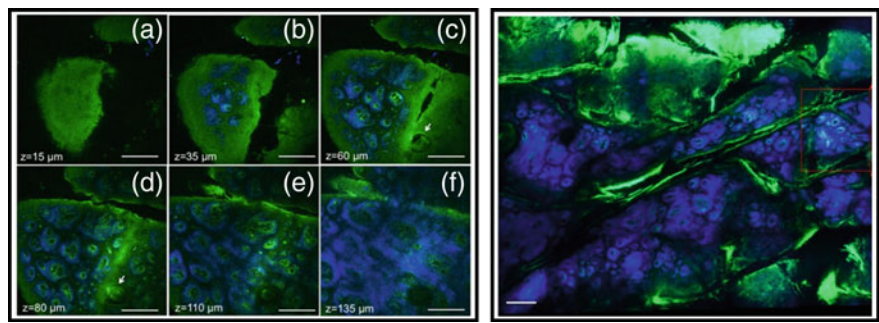
Fig. 16.6 TPM images of human skin. Colour coding green: autofluorescence from cells, blue: collagen. Left: Images of skin at different depths. Close to the surface keratin is well visible (green), and some cellular components are less visible (green punctuate) while deeper dermal papillae (blue) become visible. Scale bar is 200 μm. Right: A wide-area field of view (3.1 × 2.5 mm²) of dermo-epidermal junction, the region where skin folds are deep enough to the level of papillary dermis. Scale bar is 0.25 mm. Adapted from [58]

Fig. 16.7 Morphological and functional differences are detected in in vivo endogenous TPEF images of normal and cancerous human epithelia. Adapted from [52]

16.4.3.4 Intravital Imaging with Two-Photon Microscopy

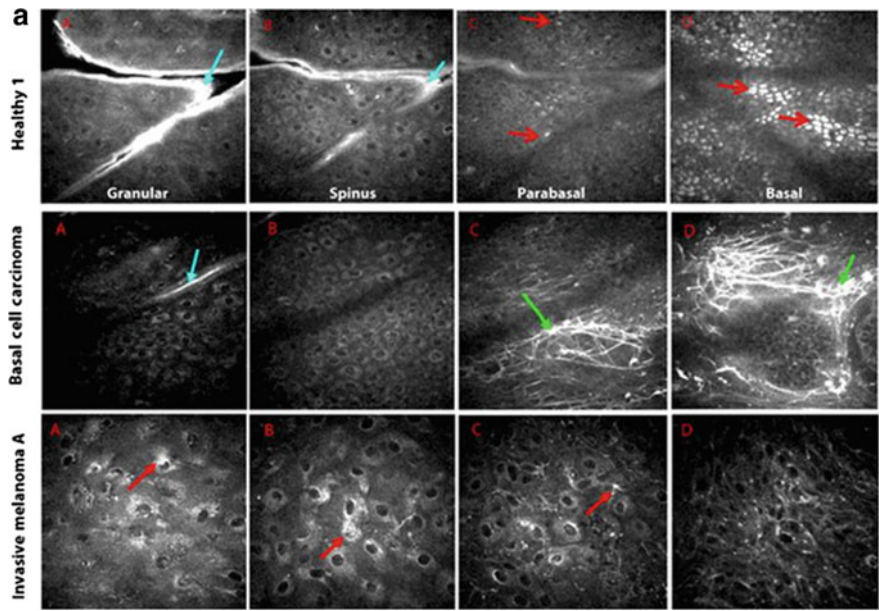The ability for deep penetration and relatively reduced photodamage/photobleaching has made TPM the technique of choice for intravital imaging of small rodents such as mice and rats. Its potential applications in intravital imaging have been recognized since early times [64]. It can be used in a non-invasive way when imaging external organs such as skin, but for imaging non-superficial organs a certain degree of invasiveness is required. A general protocol requires that the animal must be anaesthetized, where subsequently a minimal surgical intervention to expose the organ of interest follows. Such organs can be the bladder [65], the carotid [66], the gastrointestinal tract [67], and others [68]. A more elaborate method to monitor a region of interest for longer periods is to attach a glass window on the region of interest. Especially in the field of brain imaging, a cranial window is permanently attached to the scalp of mice and multiple imaging session can be performed over the course of several months [69], and even in freely moving animals [70] (Fig. 16.8).

One consideration when imaging intravitally is motion artefacts and speed. Traditional scanning methods with frame rates above 1 frame per second (fps) are too slow for acquiring static images. One has to consider the normal breathing patterns of the animal, as well as the cardiovascular pulsing. To overcome this problem without significant improvement in speed, the solution of triggered imaging has been suggested, where a monitor observes both heart rate and breathing rate and at appropriate time the trigger to image is sent [71]. Although this technique is practical, it is not real time and is not fast enough. Another method to overcome this problem is to increase the scanning speed. In this regime, there are two solutions: (a) use of a resonant scanner and (b) use of multi-spot beam [72, 73]. Resonant scanners are very fast galvo-scanners operating at a fixed speed which can acquire images with video rate [74] and higher. This has allowed intravital imaging
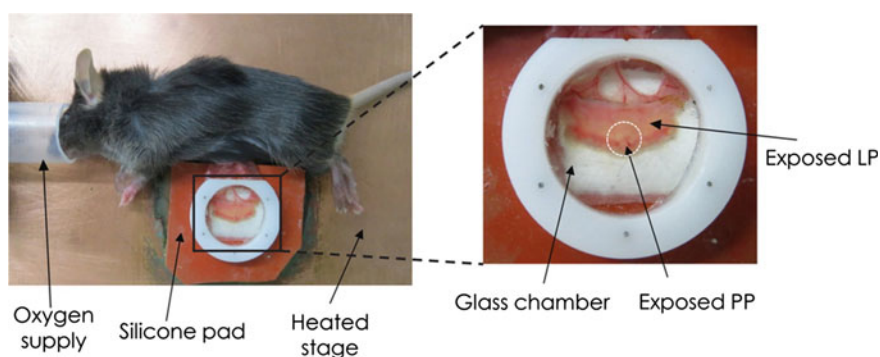

Fig. 16.8 TPM intravital imaging of gastrointestinal tract. The organ is exposed and mounted on an optical window, while the animal is anaesthetized. This can also be done with windows for tumour imaging. Adapted from [67]

with very good results. One consideration is that noise levels are high; therefore, this has to be compensated by using high concentration of dyes, and/or increasing excitation intensity. The use of hybrid detectors certainly reduces noise levels and is favoured when available. The other possibility of going faster is to use the multi-spot beam. In this case, the single laser beam is divided into many beams, typically 8–64 beams, which scan the sample simultaneously, therefore reducing scanning time 8–64-fold. In multi-spot TPM, instead of a point detector such as a PMT, a camera is used to collect the spatially separated signal. Cameras have a higher detection efficiency (or quantum efficiency—QE) compared to PMTs (Camera QE: ∼90%, PMTs QE: ∼40%). However, going deeper usually is accompanied by higher degrees of scattering and as a result signal from adjacent beams are detected. This introduces artefacts and limits the achievable resolution deeper in tissues.

Tumour growth is dynamic and takes place at variable rates and with different mechanisms [75, 76]. To elucidate the dynamics of these processes, an in vivo model is crucial. Several applications using in vivo environments by either using engineered tissue or small animal have been reported. To image the dynamic growth of cancer and invasion, Koehl et al. developed a modified skin-fold chamber model for orthotopic implantation in mice and subsequent injection of a solid cancer cell pellet [77]. They were able to monitor a slow and linear pre-angiogenic tumour growth phase at the beginning which was followed by rapid growth afterwards. They used an additional laser line at 1100 nm for imaging a near-infrared dextran variant which was helpful in separating its signal from EGFP to DsRed2. They were able to image vessels, cellular morphology, and nuclear states. Dondossola et al. using TPM and an imaging window investigated the osteolytic progression of cancer tumours on mice models and reported on the reduction of osteoclast kinetics and osteolysis, with no effect on tumour growth after bisphosphonate treatment [78]. Studies on cancer tissue such as on breast cancer [79, 80], cancer cells in vivo [81, 82], murine cutaneous squamous cell carcinoma [83], glioblastoma [84], tumour microcirculation [85], and melanoma cells [86] have been reported on intravital imaging. Several pathways for cell migration and therapy have been investigated with intravital TPM [87, 88].

16.4.3.5 Second Harmonic Generation Imaging of Collagen

SHG is an efficient label-free method for imaging collagen [89]. Apart as a contrast for visualizing the extension of extracellular matrix in connective tissue, the evolution and morphological alterations of collagen matrix have been shown to correlate with tumour growth and metastasis [18, 90]. Such changes involve collagen synthesis, increases in organization, and compaction of collagen fibres and change in their diameter. Such changes have been observed in different malignancies, and several quantification tools [91] have been proposed which could be useful for future diagnostic purposes and possibly automatic classification.

16.4.3.6 Higher Order Fluorescence and Harmonics

In the field of non-linear microscopy, the applications of three-photon excitation and third harmonic generation have been explored [92]. The advantage of three-photon excitation is that a more red-shifted laser line is required (~ 1200 nm), which allows deeper penetration inside tissues, while the emission profile of fluorophores does not change. However, higher intensities are required, and photobleaching rate can become significant. Third harmonic generation offers contrast on refractive index changes. Therefore, it provides contrast on interfaces in tissue with change in refractive index, such as the presence of membranes, blood cells, fat, and tissue layers. Together, this technique combined with TPM and SHG provides a full arsenal of tools for imaging tissue with as many details as possible [93, 94]. In practice, this allows for label-free imaging of tumour cells, red blood cells, macrophages, adipocytes, connective tissue, and the surrounding microvasculature of tissue and tumour microenvironment. Three-photon imaging has allowed imaging even through intact skull [95], and short femtosecond pulsed lasers optimized for exciting GFPs and RFPs have been demonstrated for deep tissue imaging [96] (Fig. 16.9).
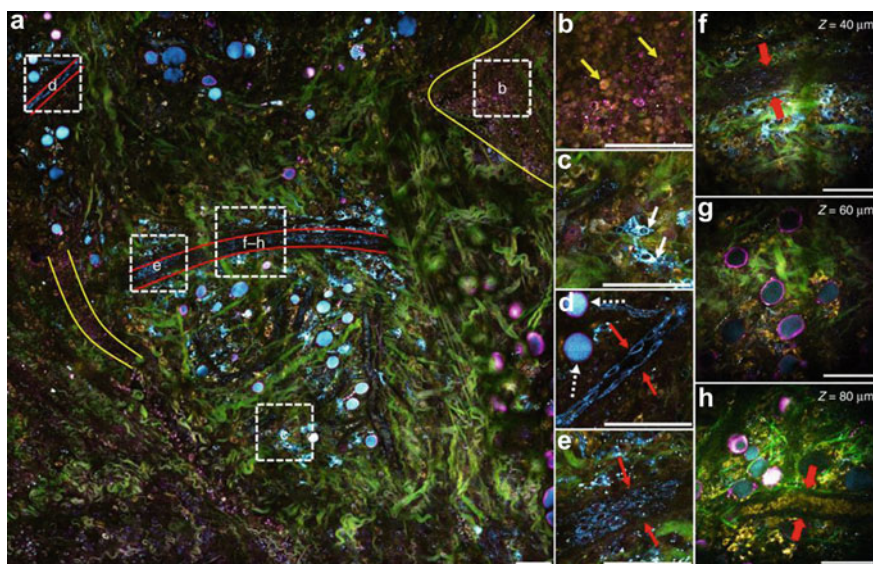
Fig. 16.9 Large field of view image (1.5×1.5 mm^2) of label-free multi-harmonic image of in vivo rat mammary tumour microenvironment. Colour coding, Green: SHG (collagen fibres), Magenta: THG (from interfaces- membranes); Yellow: two-photon excited fluorescence (mainly FAD in cells); Cyan: three-photon excited fluorescence (mainly NADH in cells). Connective tissue appears green, macrophages appear cyan with a magenta boundary and can also be identified by their morphology, tumour cells appear yellow with magenta boundary and within tumour regions magenta punctuate originating from tumour-associated vesicles are visible. Scale bar: 100 μm. Adapted from [94]

Another application to increase penetration depth and speed is wide-field two-[97, 98] and three-photon excitation [99]. Wide-field illumination ensures increased speed (frame rates of 100 Hz), since the sample is not scanned but illuminated in a similar manner as in wide-field microscopy. The apparent advantage in speed, however, is offset but reduced axial resolution, but in application such as optogenetics where speed is more important, compromise in resolution is welcome. The combination with three-photon excitation can increase penetration depth to 700 μm [99] without photodamage.

16.4.3.7 Endomicroscopy

So far, the potential and requirements of TPM have been described in detail. The potential of in vivo use has been demonstrated in small animals and in human skin imaging. If the technique were to be translated to the clinical setting, a miniaturization process is necessary. For this reason, efforts to convert this method to endomicroscopy have been made. The main difficulty has been the miniaturization of the lens and scanning head. In modern applications, this was achieved by the use of the gradient-index (GRIN) lens [57], where gradients in refractive index are used to focus light. Although this offers a compact solution for TPM, it poses a problem because chromatic aberration is significant between excitation and emission light. More recently, custom-made miniature lenses that can integrate diffractive elements [100, 101] (Fig. 16.10) have been proposed to compensate for aberrations. Scanning is performed in the miniaturized probe tip by using a piezoelectric ceramic tube [102, 103].

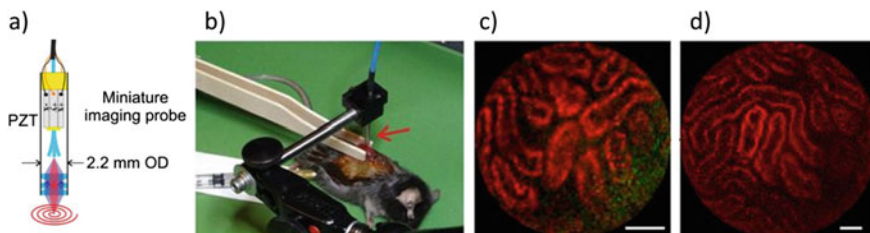**Fig. 16.10** Tip of a fibre-optic scanning two-photon endo-microscope. **a** The tip includes a piezoelectric element (PZT) for circular scanning, a miniature objective and is around 2 mm wide. **b** Anaesthetized mouse during endomicroscopic imaging. **c** TPM image of kidney, red autofluorescence, green collagen—SHG. **d** Same as in **c** but larger field of view, 450 μm. Scale bars, 50 μm. Adapted from [100]

16.4.4 Super-Resolution Microscopy

Several applications investigating oncological molecular process in this new range of resolution have been reported [104]. Resolution is very much improved in STED, but this is accompanied with reduced field of view and penetration depth. Therefore, STED is optimal when imaging molecular processes in subcellular level on cell cultures of primary or immortalized cell lines. In cancer research, some examples include imaging of ovarian cancer cells [105], rectal cancer [106] (Fig. 16.11), metastasizing cells [107], or the visualization of vimentin collapse [108] which is correlated with reduced cancer cell stiffness.

SMLM techniques have also been used in oncology studies. They constitute an obvious super-resolution alternative to confocal microscopy as they share similar limitations of sample thickness but offer one order of magnitude improved resolution. CLSM resolution is ∼200 nm while with SMLM it can be 20 nm. SMLM was effectively used to re-image archived formalin-fixed paraffin-embedded samples of breast cancer tissue. This technique was used to investigate ultrastructural features of mitochondria and nuclei, not visible with conventional techniques [109] (Fig. 16.12). This method holds potential for investigating already archived tissue samples that could be used for investigating new parameters in diagnostic procedures.

SIM has also been used in oncology research. As with previous techniques, it has also been used in imaging biopsy tissue section of benign and malignant tissue. In a study on prostate cancer tissue slides, it was shown that application of fast
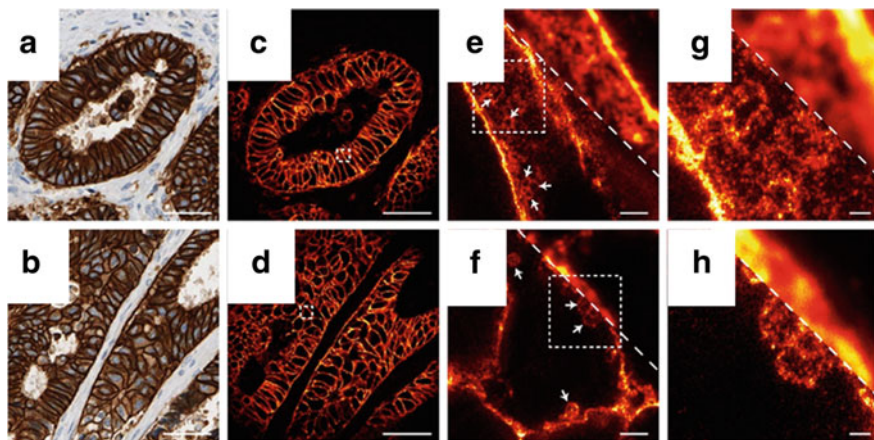

Fig. 16.11 Imaging of deparaffinized tissue slices of breast cancer tissue with conventional wide-field microscopy **a** and **b**, confocal **c–d**, **e**, **f** Magnified insets from **c** and **f**. **g** and **h** further magnification of (**e**), (**f**) Adapted from [106]
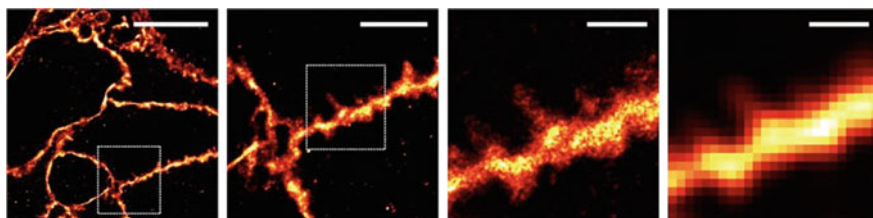
Fig. 16.12 SMLM images of HER2-positive cancer cells. The protrusions of the extracellular membrane are better visible in the SMLM images. From left to right increasing magnification insets (scale bars from left to right 10, 4, 1 to 1 μm). Last image in right is the conventional confocal microscopy image. Adapted from [109]

staining with acridine orange can produce images with similar contrast to that of Haematoxylin and Eosin (H&E). Such images feature super-resolution and additionally mosaics of the entire tissue section is possible with video-rate acquisition [110] (Fig. 16.13).

16.4.5 Multimodal Techniques

All these fluorescence-based techniques can offer new insight to different processes in the oncology field, but they can also be combined with another fluorescence-based technique to improve resolution or penetration or be combined with methods based on different contrast mechanisms.

In the field of skin imaging, confocal microscopy was combined with optical coherence tomography [111] (OCT), in a hand-held implementation [112], to detect margins of basal cell carcinoma in vivo, with the possibility of translating this technique in the clinic for diagnostic purposes. Two-photon microscopy was combined with coherent anti-Stokes Raman spectroscopy (CARS) a scattering-based method that can offer good visualization of lipids, for imaging tumour microenvironment and tracking of tumour cells and margins [113].

TPM was further combined with SIM. This combination offers the advantage of deeper penetration of the TPM beam and improved resolution offered by SIM. This multimodal technique was further combined with multifocal excitation in order to increase the speed of acquisition. This resulted in fast imaging with super-resolution of thick scattering samples such as C. Elegans embryos, Drosophila Melanogaster larval salivary glands, mouse liver tissue, and fast process in live zebrafish embryos [114–116].
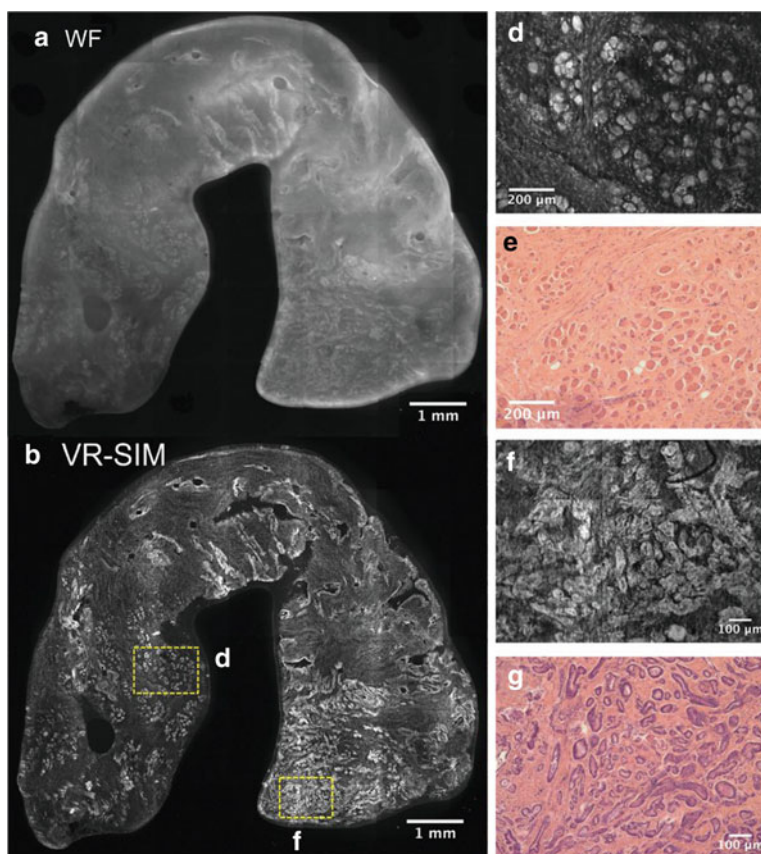
Fig. 16.13 SIM images of prostate cancer tissue section. **a** Wide-field and **b** the same section with SIM. Increase contrast is achieved with acridine orange staining. Magnified insets of **b** in **d–g** **c** and **d** areas of normal skeletal muscle and fibrous stroma. **f** and **g** depict areas of malignant glands. **d** and **f** SIM images. **e** and **g** H&E staining. Adapted from [110]

TPM microscopy has been also combined with optoacoustic imaging [117]. Two-photon images can be overlaid with optoacoustic images, resulting from the ultrasound signal due to the absorption of light at the focus of the objective, and offer contrast on vasculature and melanoma cells in vivo [118]. Such hybrid applications combine the advantages of TPM in deep penetration and high resolution with increased detection efficiency at deeper layers of tissue (Table 16.1).

Table 16.1 Characteristics of imaging techniques

	In vivo	Penetration depth	Resolution radial (XY)/axial (Z)	Label-free	Acquisition speed
TPM	Yes	200 μm	500/1500 nm	Yes	Video rate
CLSM/reflectance CLSM	Yes	50 μm/100 μm	250/750 nm–500/1500 nm	No/Yes	Video rate
LSM	Yes	50 μm/1–4 mm (in cleared samples)	1/1 μm	No	Video rate
STED	Yes	50 μm	70/120 nm	No	Video rate
SMLM	No	1–2 μm	20/100 nm	No	Seconds to minutes per frame
SIM	Yes	100 μm	120/400 nm	No	Video rate

16.5 Conclusion

Developments in advanced optical microscopy are fast. A whole plethora of techniques, all with their specific advantages, disadvantages, strongholds, and applications, is already available. Undoubtedly, new developments will come up, such as the combination of expansion and super-resolution microscopy. What we hope to have clarified is the enormous potential of advanced optical microscopy, both in fundamental research and in a more (pre)clinical setting. In that respect, especially interesting is the translation of these techniques to the clinic, e.g. by using micro-endoscopy or microscopy-at-the bedside. It definitely is worthwhile to look beyond gold standards and broadly applied techniques towards new developments.

References

1. Orlova A et al (2006) Tumor imaging using a picomolar affinity HER2 binding affibody molecule. Cancer Res 66:4339–4348
2. Holliger P, Hudson PJ (2005) Engineered antibody fragments and the rise of single domains. Nat Biotechnol 23:1126–1136
3. Keppler A et al (2003) A general method for the covalent labeling of fusion proteins with small molecules in vivo. Nat Biotechnol 21:86–89
4. Liss V, Barlag B, Nietschke M, Hensel M (2015) Self-labelling enzymes as universal tags for fluorescence microscopy, super-resolution microscopy and electron microscopy. Sci Rep 5
5. Chozinski TJ, Gagnon LA, Vaughan JC (2014) Twinkle, twinkle little star: photoswitchable fluorophores for super-resolution imaging. FEBS Lett 588:3603–3612
6. Van De Linde S et al (2011) Direct stochastic optical reconstruction microscopy with standard fluorescent probes. Nat Protoc 6:991–1009
7. Pawley JB (2006) Handbook of biological confocal microscopy, 3rd edn. https://doi.org/10.1007/978-0-387-45524-2

8. Dobbs J et al (2015) Confocal fluorescence microscopy for rapid evaluation of invasive tumor cellularity of inflammatory breast carcinoma core needle biopsies. Breast Cancer Res Treat 149:303–310
9. Huisken J, Swoger J, Del Bene F, Wittbrodt J, Stelzer E. HK (2004) Optical sectioning deep inside live embryos by selective plane illumination microscopy. Science 305:1007–1009
10. Method of the Year 2014 (2014) Nat Methods 12:1
11. Keller PJ, Dodt HU (2012) Light sheet microscopy of living or cleared specimens. Curr Opin Neurobiol 22:138–143
12. Chen BC et al (2014) Lattice light-sheet microscopy: imaging molecules to embryos at high spatiotemporal resolution. Science 346
13. Liu TL et al (2018) Observing the cell in its native state: imaging subcellular dynamics in multicellular organisms. Science. https://doi.org/10.1126/science.aaq1392
14. Denk W, Strickler JH, Webb WW (1990) Two-photon laser scanning fluorescence microscopy. Science 248:73–76
15. Masters BR, So PTC, Gratton E (1997) Multiphoton excitation fluorescence microscopy and spectroscopy of in vivo human skin. Biophys J 72:2405–2412
16. Helmchen F, Denk W (2005) Deep tissue two-photon microscopy. Nat Methods 2:932–940
17. Patterson GH, Piston DW (2000) Photobleaching in two-photon excitation microscopy. Biophys J 78:2159–2162
18. Perry SW, Burke RM, Brown EB (2012) Two-photon and second harmonic microscopy in clinical and translational cancer research. Ann Biomed Eng 40:277–291
19. Liu J (2015) Two-photon microscopy in pre-clinical and clinical cancer research. Front Optoelectron 8:141–151
20. Condeelis J, Weissleder R (2010) In vivo imaging in cancer. Cold Spring Harbor Perspect Biol 2
21. Provenzano PP, Eliceiri KW, Keely PJ (2009) Multiphoton microscopy and fluorescence lifetime imaging microscopy (FLIM) to monitor metastasis and the tumor microenvironment. Clin Exp Metas 26:357–370
22. Konig K (2000) Multiphoton microscopy in life sciences. J Microsc 200:83–104
23. Wang BG, Konig K, Halbhuber KJ (2010) Two-photon microscopy of deep intravital tissues and its merits in clinical research. J Microsc 238:1–20
24. Staughton TJ, McGillicuddy CJ, Weinberg PD (2001) Techniques for reducing the interfering effects of autofluorescence in fluorescence microscopy: improved detection of sulphorhodamine B-labelled albumin in arterial tissue. J Microsc 201:70–76
25. Hell SW (2009) Microscopy and its focal switch. Nat Methods 6:24–32
26. Betzig E et al (2006) Imaging intracellular fluorescent proteins at nanometer resolution. Science 313:1642–1645
27. Rust MJ, Bates M, Zhuang X (2006) Sub-diffraction-limit imaging by stochastic optical reconstruction microscopy (STORM). Nat Methods 3:793–795
28. Gustafsson MGL (2000) Surpassing the lateral resolution limit by a factor of two using structured illumination microscopy. J Microsc 198:82–87
29. Heintzmann R, Huser T (2017) Super-resolution structured illumination microscopy. Chem Rev 117:13890–13908
30. Heintzmann R, Jovin TM, Cremer C (2002) Saturated patterned excitation microscopy—a concept for optical resolution improvement. J Opt Soc Am A 19:1599
31. Gustafsson MGL (2005) Nonlinear structured-illumination microscopy: wide-field fluorescence imaging with theoretically unlimited resolution. Proc Natl Acad Sci 102:13081–13086
32. Vermeulen L et al (2013) Defining stem cell dynamics in models of intestinal tumor initiation. Science 342:995–998
33. Denais CM et al (2016) Nuclear envelope rupture and repair during cancer cell migration. Science 352:353–358
34. Shimokawa M et al (2017) Visualization and targeting of LGR5 + human colon cancer stem cells. Nature 545:187–192

35. Que S (2015) Non-invasive imaging technologies for the delineation of basal cell carcinomas. J Invest Dermatol 135:S32
36. Que SKT (2015) Research techniques made simple: noninvasive imaging technologies for the delineation of basal cell carcinomas. J Investig Dermatol 136:e33–e38
37. Schiffhauer LM et al (2009) Confocal microscopy of unfixed breast needle core biopsies: a comparison to fixed and stained sections. BMC Cancer 9
38. Tanaka N et al (2017) Whole-tissue biopsy phenotyping of three-dimensional tumours reveals patterns of cancer heterogeneity. Nat Biomed Eng 1:796–806
39. Uhlén P, Tanaka N (2018) Improved pathological examination of tumors with 3D light-sheet microscopy. Trends Cancer 4:337–341
40. Glaser AK et al (2017) Light-sheet microscopy for slide-free non-destructive pathology of large clinical specimens. Nat Biomed Eng 1
41. Matsui T et al (2017) Non-labeling multiphoton excitation microscopy as a novel diagnostic tool for discriminating normal tissue and colorectal cancer lesions. Sci Rep 7
42. Cicchi R et al (2010) Time- and Spectral-resolved two-photon imaging of healthy bladder mucosa and carcinoma in situ. Opt Express 18:3840–3849
43. Wu X et al (2013) Label-free detection of breast masses using multiphoton microscopy. PLoS One 8
44. Skala MC et al (2007) In vivo multiphoton microscopy of NADH and FAD redox states, fluorescence lifetimes, and cellular morphology in precancerous epithelia. Proc Natl Acad Sci USA 104:19494–19499
45. Ostrander JH et al (2010) Optical redox ratio differentiates breast cancer cell lines based on estrogen receptor status. Cancer Res 70:4759–4766
46. Liu Z et al (2018) Mapping metabolic changes by noninvasive, multiparametric, high-resolution imaging using endogenous contrast. Sci Adv 4
47. Huang S, Heikal AA, Webb WW (2002) Two-photon fluorescence spectroscopy and microscopy of NAD(P)H and flavoprotein. Biophys J 82:2811–2825
48. Alhallak K et al (2016) Optical redox ratio identifies metastatic potential-dependent changes in breast cancer cell metabolism. Clin Oncol 34:2303–2311
49. Patalay R et al (2011) Quantification of cellular autofluorescence of human skin using multiphoton tomography and fluorescence lifetime imaging in two spectral detection channels. Biomed Opt Express 2:3295–3308
50. Stringari C, Nourse JL, Flanagan LA, Gratton E (2012) Phasor fluorescence lifetime microscopy of free and protein-bound NADH reveals neural stem cell differentiation potential. PLoS ONE. https://doi.org/10.1371/journal.pone.0048014
51. Stuntz E et al (2017) Endogenous two-photon excited fluorescence imaging characterizes neuron and astrocyte metabolic responses to manganese toxicity/631/378/1689/364/639/624/1111/55/14/69/14/63/123 article. Sci Rep. https://doi.org/10.1038/s41598-017-01015-9
52. Pouli D et al (2016) Imaging mitochondrial dynamics in human skin reveals depth-dependent hypoxia and malignant potential for diagnosis. Sci Transl Med 8
53. So P, Kim H, Kochevar I (1998) Two-photon deep tissue ex vivo imaging of mouse dermal and subcutaneous structures. Opt Express 3:339–350
54. Konig K, Riemann I (2003) High-resolution multiphoton tomography of human skin with subcellular spatial resolution and picosecond time resolution. J Biomed Opt 8:432–439
55. König K, Konig K (2008) Clinical multiphoton tomography. J Biophotonics 1:13–23
56. Breunig HG, Studier H, Konig K (2010) Multiphoton excitation characteristics of cellular fluorophores of human skin in vivo. Opt Express 18:7857–7871
57. König K et al (2007) Clinical two-photon microendoscopy. Microsc Res Tech 70:398–402
58. Balu M, Mikami H, Hou J, Potma EO, Tromberg BJ (2016) Rapid mesoscale multiphoton microscopy of human skin. Biomed Opt Express 7:4375
59. Heuke S et al (2013) Detection and discrimination of non-melanoma skin cancer by multimodal imaging. Healthcare 1:64–83

60. Balu M et al (2015) In vivo multiphoton microscopy of basal cell carcinoma. JAMA Dermatol 151:1068–1074
61. Cicchi R et al (2007) Multidimensional non-linear laser imaging of basal cell carcinoma. Opt Express 15:10135
62. Patalay R et al (2012) Multiphoton multispectral fluorescence lifetime tomography for the evaluation of basal cell carcinomas. PLoS One 7
63. Seidenari S et al (2013) Multiphoton laser tomography and fluorescence lifetime imaging of melanoma: morphologic features and quantitative data for sensitive and specific non-invasive diagnostics. PLoS One 8:e70682
64. Flesken-Nikitin A, Williams RM, Zipfel WR, Webb WW, Nikitin AY (2004) Use of multiphoton imaging for studying cell migration in the mouse. Methods Mol Biol 294(335–46):335–346
65. Sano T et al (2016) Intravital imaging of mouse urothelium reveals activation of extracellular signal-regulated kinase by stretch-induced intravesical release of ATP. Physiol Rep 4
66. Wu Z et al (2017) Multi-photon microscopy in cardiovascular research. Methods 130:79–89
67. Kolesnikov M, Farache J, Shakhar G (2015) Intravital two-photon imaging of the gastrointestinal tract. J Immunol Methods 421:73–80
68. Wyckoff J, Gligorijevic B, Entenberg D, Segall J, Condeelis J (2011) High-resolution multiphoton imaging of tumors in vivo. Cold Spring Harb Protoc 6:1167–1184
69. Drew PJ et al (2010) Chronic optical access through a polished and reinforced thinned skull. Nat Methods 7:981–984
70. Sawinski J et al (2009) Visually evoked activity in cortical cells imaged in freely moving animals. Proc Natl Acad Sci 106:19557–19562
71. Megens RTA et al (2010) In vivo high-resolution structural imaging of large arteries in small rodents using two-photon laser scanning microscopy. J Biomed Opt 15:11108
72. Bewersdorf J, Pick R, Hell SW (1998) Multifocal multiphoton microscopy. Opt Lett 23:655
73. Niesner R, Andresen V, Neumann J, Spiecker H, Gunzer M (2007) The power of single and multibeam two-photon microscopy for high-resolution and high-speed deep tissue and intravital imaging. Biophys J 93:2519–2529
74. Kirkpatrick N et al (2012) Video-rate resonant scanning multiphoton microscopy: an emerging technique for intravital imaging of the tumor microenvironment. IntraVital 1:60–68
75. Condeelis J, Segall JE (2003) Intravital imaging of cell movement in tumours. Nat Rev Cancer 3:921–930
76. Friedl P, Gilmour D (2009) Collective cell migration in morphogenesis, regeneration and cancer. Nat Rev Mol Cell Biol 10:445–457
77. Alexander S, Koehl GE, Hirschberg M, Geissler EK, Friedl P (2008) Dynamic imaging of cancer growth and invasion: a modified skin-fold chamber model. Histochem Cell Biol 130:1147–1154
78. Dondossola E et al (2018) Intravital microscopy of osteolytic progression and therapy response of cancer lesions in the bone. Sci Transl Med 10
79. Ilina O et al (2018) Intravital microscopy of collective invasion plasticity in breast cancer. Dis Model Mech 11
80. Patsialou A et al (2013) Intravital multiphoton imaging reveals multicellular streaming as a crucial component of in vivo cell migration in human breast tumors. IntraVital 2:e25294
81. Le Dévédec SE et al (2011) Two-photon intravital multicolour imaging to study metastatic behaviour of cancer cells in vivo. Methods Mol Biol. https://doi.org/10.1007/978-1-61779-207-6_22
82. Koga S et al (2014) In vivo subcellular imaging of tumors in mouse models using a fluorophore-conjugated anti-carcinoembryonic antigen antibody in two-photon excitation microscopy. Cancer Sci 105:1299–1306

83. Thomas G et al (2014) In vivo nonlinear spectral imaging as a tool to monitor early spectroscopic and metabolic changes in a murine cutaneous squamous cell carcinoma model. Biomed Opt Express 5:4281

84. Kantelhardt SR et al (2016) In vivo multiphoton tomography and fluorescence lifetime imaging of human brain tumor tissue. J Neurooncol 127:473–482

85. Lunt SJ, Gray C, Reyes-Aldasoro CC, Matcher SJ, Tozer GM (2010) Application of intravital microscopy in studies of tumor microcirculation. J Biomed Opt 15:011113

86. Bentolila NY, Barnhill RL, Lugassy C, Bentolila LA (2018) Intravital imaging of human melanoma cells in the mouse ear skin by two-photon excitation microscopy. In: Damoiseaux R, Hasson S (eds) BT—reporter gene assays: methods and protocols. Springer, New York, pp 223–232. https://doi.org/10.1007/978-1-4939-7724-6_15

87. Alexander S, Weigelin B, Winkler F, Friedl P (2013) Preclinical intravital microscopy of the tumour-stroma interface: invasion, metastasis, and therapy response. Curr Opin Cell Biol 25:659–671

88. Beerling E, Ritsma L, Vrisekoop N, Derksen PWB, van Rheenen J (2011) Intravital microscopy: new insights into metastasis of tumors. J Cell Sci 124:299–310

89. Chen X, Nadiarynkh O, Plotnikov S, Campagnola PJ (2012) Second harmonic generation microscopy for quantitative analysis of collagen fibrillar structure. Nat Protoc 7:654–669

90. Provenzano PP et al (2006) Collagen reorganization at the tumor-stromal interface facilitates local invasion. BMC Med 4

91. Tilbury K, Campagnola PJ (2015) Applications of second-harmonic generation imaging microscopy in ovarian and breast cancer. Perspect Med Chem 7:21–32

92. Horton NG et al (2013) In vivo three-photon microscopy of subcortical structures within an intact mouse brain. Nat Photonics 7:205–209

93. Weigelin B, Bakker G-J, Friedl P (2012) Intravital third harmonic generation microscopy of collective melanoma cell invasion. IntraVital 1:32–43

94. You S et al (2018) Intravital imaging by simultaneous label-free autofluorescence-multiharmonic microscopy. Nat Commun 9

95. Wang T et al (2018) Three-photon imaging of mouse brain structure and function through the intact skull. Nat Methods 15:789–792

96. Guesmi K et al (2018) Dual-color deep-tissue three-photon microscopy with a multiband infrared laser. Light Sci Appl 7

97. Hwang JY et al (2011) Multimodal wide-field two-photon excitation imaging: characterization of the technique for in vivo applications. Biomed Opt Express 2:356

98. Cheng L-C et al (2012) Spatiotemporal focusing-based widefield multiphoton microscopy for fast optical sectioning. Opt Express 20:8939

99. Rowlands CJ et al (2017) Wide-field three-photon excitation in biological samples. Light Sci Appl 6

100. Ducourthial G et al (2015) Development of a real-time flexible multiphoton microendoscope for label-free imaging in a live animal. Sci Rep 5

101. Liang W, Hall G, Messerschmidt B, Li MJ, Li X (2017) Nonlinear optical endomicroscopy for label-free functional histology in vivo. Light Sci Appl 6

102. Kundrat MJ, Reinhall PG, Lee CM, Seibel EJ (2011) High performance open loop control of scanning with a small cylindrical cantilever beam. J Sound Vib 330:1762–1771

103. Zhao Y, Nakamura H, Gordon RJ (2010) Development of a versatile two-photon endoscope for biological imaging. Biomed Opt Express 1:1159

104. Blom H, Widengren J (2017) Stimulated emission depletion microscopy. Chem Rev 117:7377–7427

105. Sharma S et al (2012) Correlative nanomechanical profiling with super-resolution F-actin imaging reveals novel insights into mechanisms of cisplatin resistance in ovarian cancer cells. Nanomedicine Nanotechnol Biol Med. https://doi.org/10.1016/j.nano.2011.09.015

106. Ilgen P et al (2014) STED super-resolution microscopy of clinical paraffin-embedded human rectal cancer tissue. PLoS One 9

107. Rönnlund D, Gad AKB, Blom H, Aspenström P, Widengren J (2013) Spatial organization of proteins in metastasizing cells. Cytom Part A 83:855–865
108. Rathje L-SZ et al (2014) Oncogenes induce a vimentin filament collapse mediated by HDAC6 that is linked to cell stiffness. Proc Natl Acad Sci 111:1515–1520
109. Creech MK, Wang J, Nan X, Gibbs SL (2017) Superresolution imaging of clinical formalin fixed paraffin embedded breast cancer with single molecule localization microscopy. Sci Rep 7
110. Wang M et al (2015) High-resolution rapid diagnostic imaging of whole prostate biopsies using video-rate fluorescence structured illumination microscopy. Cancer Res 75:4032–4041
111. Wang J, Xu Y, Boppart SA (2017) Review of optical coherence tomography in oncology. J Biomed Opt 22:1
112. Iftimia N et al (2017) Handheld optical coherence tomography–reflectance confocal microscopy probe for detection of basal cell carcinoma and delineation of margins. J Biomed Opt 22:076006
113. Lee M et al (2015) In vivo imaging of the tumor and its associated microenvironment using combined CARS/2-photon microscopy. IntraVital 4:e1055430
114. Andresen, V. et al. High-Resolution Intravital Microscopy. PLoS One 7, (2012)
115. York AG et al (2012) Resolution doubling in live, multicellular organisms via multifocal structured illumination microscopy. Nat Methods 9:749–754
116. Ingaramo M et al (2014) Two-photon excitation improves multifocal structured illumination microscopy in thick scattering tissue. Proc Natl Acad Sci 111:5254–5259
117. Tserevelakis GJ, Soliman D, Omar M, Ntziachristos V (2014) Hybrid multiphoton and optoacoustic microscope. Opt Lett 39:1819
118. Kellnberger S et al (2018) Optoacoustic microscopy at multiple discrete frequencies. Light Sci Appl 7:109